MNRAS 000, 1–5 (2017) Preprint 24 March 2017 Compiled using MNRAS LATEX style file v3.0

The cosmic microwave background Cold Spot anomaly: the impact of sky masking and the expected contribution from the Integrated Sachs-Wolfe

Krishna Naidoo[1]★, Aurélien Benoit-Lévy[2]† and Ofer Lahav[1]‡
[1]Department of Physics & Astronomy, University College London, Gower Street, London WC1E 6BT, UK
[2]Sorbonne Universités, UPMC Univ Paris 6 et CNRS, UMR 7095, Institut d'Astrophysique de Paris, 98 bis bd Arago, 75014 Paris, France

arXiv:1703.07894v1 [astro-ph.CO] 23 Mar 2017

Accepted XXX. Received YYY; in original form ZZZ

ABSTRACT

We reanalyse the cosmic microwave background (CMB) Cold Spot (CS) anomaly with particular focus on understanding the bias a mask (to remove Galactic and point sources contamination) may introduce. We measure the coldest spot, found by applying the Spherical Mexican Hat Wavelet (SMHW) transform on 100,000 masked and unmasked CMB simulated maps. The coldest spot in masked maps is the same as in unmasked maps only 48% of the time, suggesting that false minima are more frequently measured in masked maps. Given the temperature profile of the CS, we estimate at 94% the probability that the CS is the coldest spot on the sky, making the comparison to the unmasked coldest spots appropriate. We found that the significance of the CS is $\sim 1.9\sigma$ for an angular scale $R = 5^\circ$ of the SMHW ($< 2\sigma$ for all R). Furthermore, the Integrated Sachs-Wolfe (ISW) contributes $\sim 10\%$ (mean of $\sim -10\mu K$ but consistent with zero) of the full profile of the coldest spots. This is consistent with recent ΛCDM ISW reconstructions of line of sight voids.

Key words: cosmic background radiation

1 INTRODUCTION

The cosmic microwave background (CMB) Cold Spot (CS) anomaly was discovered by Vielva et al. (2004) using the Spherical Mexican Hat Wavelet (SMHW) (Cayón et al. 2001) on WMAP data. The anomaly has persisted (Cruz et al. 2007; Bennett et al. 2011) and was later verified by Planck (Planck Collaboration et al. 2015a).

Inoue & Silk (2006, 2007) claimed the Integrated Sachs-Wolfe (ISW) (Sachs & Wolfe 1967) and Rees-Sciama (RS) (Rees & Sciama 1968) effects of a large void at redshift $z \sim 1$ could explain the entire feature (the RS is subdominant in all cases (Nadathur et al. 2014)). However pencil beam surveys (Bremer et al. 2010; Granett et al. 2010) have effectively ruled out the possibility of such a large void at high redshift (i.e. $0.5 < z < 1$). Nevertheless, studies of the galaxy distribution in the region appear to indicate a large void exists in the line of sight (LOS) at lower redshift (see Szapudi et al. 2015; Kovács & García-Bellido 2016). But, several studies have already shown that neither a single spherical/elliptical void or multiple voids are capable of explaining the full CS profile (see Nadathur et al. 2014; Zibin 2014; Marcos-Caballero et al. 2016; Naidoo et al. 2016) assuming ΛCDM. Hints of a stronger than expected ISW signal have been found in some stacked void studies (Granett et al. 2008; Cai et al. 2014; Kovács et al. 2017; Kovács 2017), leading to speculation that there may be a much greater causal relation, than predicted by the ISW, between the CS and LOS voids. However, Ilić et al. (2013), Hotchkiss et al. (2015) and Nadathur & Crittenden (2016) have found no such excess and obtain consistent results with ΛCDM.

The use of a mask in the SMHW analysis of the CS, to minimise contribution from the Galaxy and point sources, is common practice (see Vielva et al. 2004; Zhang & Huterer 2010; Nadathur et al. 2014; Planck Collaboration et al. 2015a). Because the SMHW transform integrates across the sky, contributions from masked areas will leak to neighbouring regions. Thus a more aggressive mask than the original is applied to the filtered map (see Zhang & Huterer 2010; Rassat et al. 2014). While the application of a mask is sometimes unavoidable, Rassat et al. (2014) show that many CMB anomalies, including the CS, are no longer significant when carried out without the use of a mask on full sky LGMCA CMB maps (Bobin et al. 2014). Furthermore,

★ E-mail: krishna.naidoo.11@ucl.ac.uk
† E-mail: benoitl@iap.fr
‡ E-mail: o.lahav@ucl.ac.uk

© 2017 The Authors

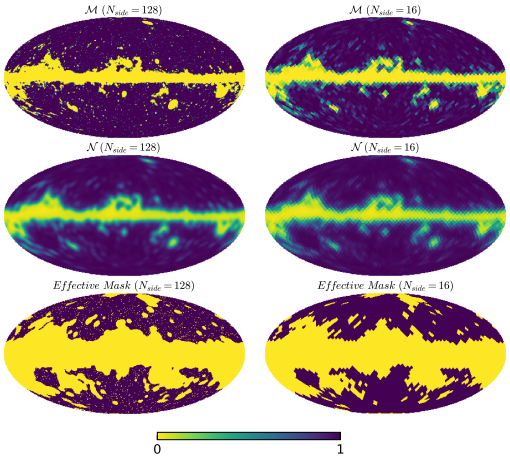

Figure 1. In the top panels the Planck Common Field mask is shown ($\mathcal{M}$), the middle panels show the derived occupancy fraction ($\mathcal{N}$) and the bottom panels show the effective mask. These are shown at $N_{side} = 128$ on the *left* and 16 on the *right*.

the CS's inability to be detected by other filters (see Zhang & Huterer 2010) has placed doubt on its significance. However, this is often argued to be due to the SMHW sensitivity to what makes the CS anomalous, i.e. its unusually high transition from cold to hot.

In this paper, we investigate the effects of masking on the detection and resulting significance of the CS and the expected contribution of the ISW to the CS profile.

2 METHOD

In the following analysis we make use of the Planck SMICA CMB map and Planck Common Field mask[1].

2.1 Spherical Mexican Hat Wavelet

The Spherical Mexican Hat Wavelet (SMHW) is defined according to an angular scale R as:

$$\Psi(\theta; R) = A_{wav}(R)\left(1 + \left(\frac{y}{2}\right)^2\right)^2\left(2 - \left(\frac{y}{R}\right)^2\right)\exp\left(-\frac{y^2}{2R^2}\right), \quad (1)$$

where $y \equiv 2\tan(\theta/2)$ and θ is the angular separation between two points, $\hat{n}$ and $\hat{n}'$, on a sphere. $A_{wav}(R)$ is a normalisation constant defined as:

$$A_{wav}(R) = \left[2\pi R^2\left(1 + \frac{R^2}{2} + \frac{R^4}{4}\right)\right]^{-1/2}. \quad (2)$$

The cumulative filtered temperature, i.e. the SMHW value of a point at $\hat{n}$ as the transform is applied to an area with an angular radius of θ, is given by:

$$\Delta T_{wav}(\theta; \hat{n}, R) = \int_0^\theta \Delta T(\vec{n}')\Psi(\theta'; R)d\Omega', \quad (3)$$

where $\hat{n}'$ are pixels located within an angular distance $< \theta$ from point $\hat{n}$. This is found by using the `HEALPix` function `query_disc`. The SMHW of a single pixel, $\Delta\mathcal{T}_\Psi(\hat{n})$, is then calculated by integrating equation 3 across the whole sky or up to an angular radius of $\theta \simeq 4R$ since $\Psi(\theta \gtrsim 4R; R) \simeq 0$.

$$\Delta\mathcal{T}_\Psi(\hat{n}) = \Delta T_{wav}(\pi; \hat{n}, R) \simeq \Delta T_{wav}(4R; \hat{n}, R) \quad (4)$$

[1] Available from http://pla.esac.esa.int/pla/#home.

In order to remove contamination from Galactic foregrounds and point sources a mask is applied. In order to do this we must first calculate an occupancy fraction (Zhang & Huterer 2010), which calculates the contribution of masked regions to the wavelet transform. This is calculated by:

$$\mathcal{N}(\hat{n}; R) \simeq \int_0^{4R} \mathcal{M}(\hat{n}')\Psi^2(\theta'; R)d\Omega', \quad (5)$$

where $\mathcal{M}(\hat{n})$ and $\mathcal{N}(\hat{n})$ are the mask and occupancy fraction value, respectively, at a point $\hat{n}$. Similarly to equation 4, we integrate only up to $\theta = 4R$ rather than $\theta = \pi$ for the exact solution since $\Psi(\theta \gtrsim 4R; R) \simeq 0$.

The SMHW is applied to the full CMB map. Pixels with a mask and occupancy fraction of $\mathcal{M} < 0.9$ or $\mathcal{N} < 0.95$, respectively, are then masked to remove areas of the map where contaminated sources may contribute significantly to the result. This means the effective mask applied to the map is considerably larger than the mask $\mathcal{M}$, with $\sim 48\%$ ($\sim 66\%$ for $\mathcal{M} > 0.9$) unmasked pixels (see figure 1).

2.2 Simulating Cosmic Microwave Background and Integrated Sachs-Wolfe maps

Using `CLASS` (Blas et al. 2011)[2] we generate C_ℓ based on best fit Planck $TT,TE,EE{+}lowP{+}lensing{+}ext$ cosmological parameters (see Planck Collaboration et al. 2015b). We deliberately turn off the late ISW effect (i.e. $z < 10$), giving C_ℓ for the primordial CMB. C_ℓ for only the late ISW effect are calculated seperately. We then generate primordial CMB maps, ΔT_P, and ISW maps, ΔT_{ISW}, using the `HEALPix` software Górski et al. (2005) at $N_{side} = 128$ and add them,

$$\Delta T(\hat{n}) = \Delta T_P(\hat{n}) + \Delta T_{ISW}(\hat{n}), \quad (6)$$

to give a full CMB map (ΔT). The motivation for generating these maps seperately is to allow us to investigate the ISW contribution to the coldest spots in CMB realisations. Since the major contribution to the ΔT_{ISW} occurs at $z < 1.4$ the correlation between ΔT_P and ΔT_{ISW} is expected to be small.

2.3 Searching for the coldest spots

To search for the coldest spots in our simulated maps we apply the SMHW transform to ΔT maps downgraded from $N_{side} = 128$ to 16. This is carried out with and without a mask. Using the location of the coldest pixel in the downgraded map ($N_{side} = 16$) we measure $\Delta T_{wav}(\theta; R)$ (where $R = 5^\circ$), $\Delta T(\theta)$ and $\Delta T_{ISW}(\theta)$ (i.e. the average ΔT_i of i in concentric rings of the coldest spot) on the original $N_{side} = 128$ map. This was carried out on 100,000 simulations.

To understand the role of masking we additionally measure the angular separation, α, of the coldest spot on the unmasked and the masked CMB. The coldest spot in unmasked maps is only considered to have been observed in masked maps if $\alpha = 0$, since even measuring it off center will introduce a bias. We apply the exact same procedure to the Planck SMICA map using the Planck Common Field mask.

A frequentist, rather than a bayesian, approach is applied as we are determining the CS consistency with ΛCDM rather than doing model comparisons where the alternative would be better suited.

[2] Software is available from http://class-code.net/.

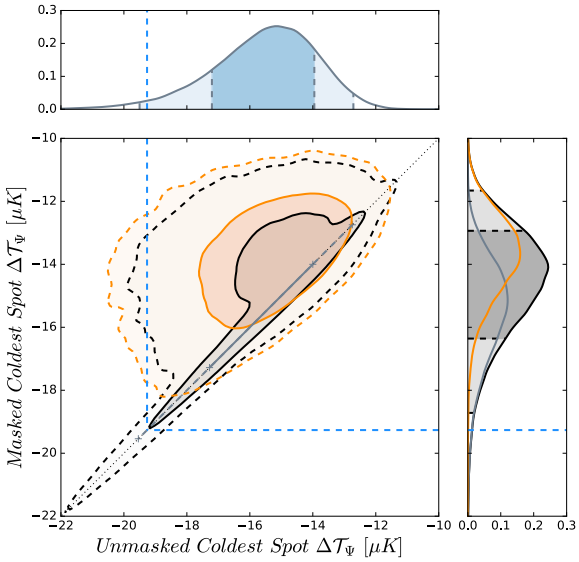

Figure 2. The relation between the unmasked and masked coldest spot's $\Delta\mathcal{T}_\Psi$ for all, real and false minima are shown in black, grey and orange respectively. The full lines and darker shaded contours indicate the 1σ (68%) regions and the dashed lines and lighter shaded contours indicate the 2σ (95%) regions. The *right* panel shows a kernal density plot of the masked, real and false minima. In the *top* panel a kernal density plot of the unmasked coldest spots is shown. Masked cold spot measurements are heavily biased due to masking effects. This is most prominent for masked $\Delta\mathcal{T}_\Psi > -18\mu K$, since false minima below this appear to be very rare. The CS's $\Delta\mathcal{T}_\Psi$ (blue dashed line) is shown for comparison to the masked and unmasked distribution.

3 RESULTS

3.1 Masked vs unmasked coldest spot

We compare the coldest spots in masked and unmasked maps in figure 2. We will refer to cases where the coldest spot in masked map is equivalent to the one found in unmasked map as real sources and cases where this is not the case as false minima. Using the Planck Common Field mask, we find that real sources are only observed ~ 48% of the time, as one would expect given that this is the effective fraction of the map that is removed from the analysis by the mask. The use of a mask biases $\Delta\mathcal{T}_\Psi$, causing it to be on average $\sim +0.93\mu K$ using the Common Field mask, while false minima are on average $\sim +1.78\mu K$ hotter than the real sources. Interestingly, for colder masked sources (i.e. $\Delta\mathcal{T}_\Psi < -18\mu K$) there seems to be very little contribution from false minima. This becomes particularly interesting for the CMB CS.

3.2 The Cold Spot in Planck data

The CS has a $\Delta\mathcal{T}_\Psi \simeq -19.3\mu K$ with a significance of $\sim 2.2\sigma$ when masked. To make a comparison between the unmasked coldest spots in simulations we must first understand whether the CS is indeed our CMB's unmasked coldest spot. Without any prior knowledge of the CS's $\Delta\mathcal{T}_\Psi$ the probability that the masked is equivalent to the unmasked coldest spot ($\mathbb{P}(\mathcal{U})$) is $\simeq 0.48$. However, the probability increases as $\Delta\mathcal{T}_\Psi$ decreases. For the CS, the conditional probability ($\mathbb{P}(\mathcal{U}|\Delta\mathcal{T}_\Psi^{CS})$) is actually $\simeq 0.94$. This means we can be fairly certain that the CS is the CMB's unmasked coldest spot. This probability was calculated by finding the fraction of the coldest spots which are real sources measured with a $\Delta\mathcal{T}_\Psi$ within a 0.5 μK bin containing the CS $\Delta\mathcal{T}_\Psi^{CS}$. In figure 2 the CS's $\Delta\mathcal{T}_\Psi$ is shown and lies well within the 2σ distribution of the unmasked coldest spots in simulations. The CS's significance in comparison to the unmasked coldest spots is $\sim 1.9\sigma$ (which corresponds to a P-value ~ 3%). In figure 3 we compare the CS's $\Delta T(\theta)$ and $\Delta T_{wav}(\theta)$ in comparison to the 1 and 2σ contours of the masked and unmasked coldest spots in simulations (indicated by black lines and blue contours respectively). The comparison illustrates precisely how the observed profiles are biased. For $\Delta T(\theta)$ the main difference occurs near the center ($\theta < 5^\circ$) where the unmasked profiles appear slightly colder in comparison. This appears to be more pronounced in $\Delta T_{wav}(\theta)$, where the distribution is found to be consistently colder for all values of θ.

3.3 The Cold Spot's significance vs. mask size

Using the SILC CMB map (Rogers et al. 2016, specifically using the $N = 5$ map) and corresponding mask we test the effect of the size of the mask on the CS's significance. The mask for the SILC CMB map is relatively small such that even the effective mask has ~ 88% unmasked pixels (f_{sky}). We gradually enlarge this mask by masking away a wider galactic strip and run the same procedure. In figure 4 we plot the CS's significance in comparison to the masked coldest spots (shown in black) and compare the CS's significance to the unmasked/real coldest spots (shown in blue) and the false minima (shown in orange) as a function of f_{sky}. The CS significance in comparison to real sources always remains $< 2\sigma$. But in comparison to the masked coldest spots the significance becomes larger as f_{sky} decreases. The significance of the CS also increases in comparison to false minima, which is found to be because their temperature increases as well. Rather unsurprisingly a larger mask will make it harder to find the real coldest spot and also make it more likely that a hotter false minima is measured. The net effect is that real sources will have a boosted significance due to the size of the mask.

3.4 The Integrated Sachs-Wolfe for the coldest spots

The ISW contribution to the coldest spots in simulations was measured and is shown in figure 5. Here we display the mean and 1σ contours for all the unmasked coldest spots and the most extreme 3% (which approximately corresponds to the CS's P-value). The profiles are poorly constrained and very similar, with the more extreme case tending to be slightly more negative. The result illustrate that it is very likely that the ISW plays a minor role in the CS profile: ~ 10% of the full profile. The reconstructed ISW profiles (Rassat et al. 2014; Nadathur et al. 2014; Finelli et al. 2016; Planck Collaboration et al. 2016) appear to be consistent with the predicted ISW shown in figure 5. The presence of prominant voids in the LOS (see Szapudi et al. 2015; Kovács & García-Bellido 2016) are therefore precisely what we would expect from ΛCDM.

3.5 Dependence on angular scale

Up to this point we have used a preselected angular scale, $R = 5^\circ$, where the CS was measured to be most significant

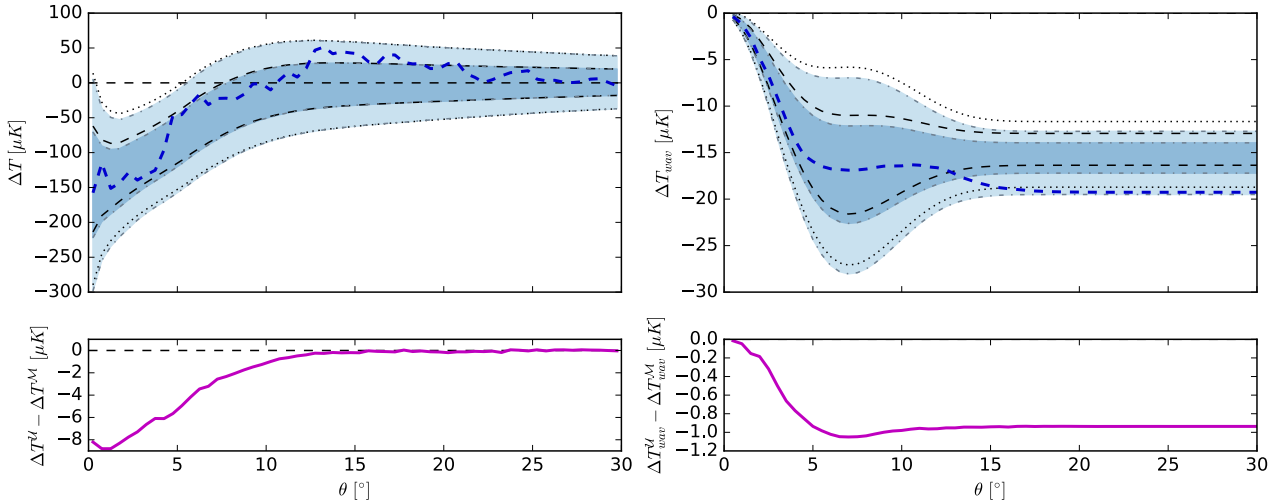
$\Delta T\ [\mu K]$
$\Delta T_{wav}\ [\mu K]$
$\Delta T^{\mathcal{U}} - \Delta T^{\mathcal{M}}\ [\mu K]$
$\Delta T^{\mathcal{U}}_{wav} - \Delta T^{\mathcal{M}}_{wav}\ [\mu K]$
$\theta\ [^\circ]$
$\theta\ [^\circ]$

Figure 3. The 1 and 2σ contours (dark and light shades, respectively) for the $\Delta T(\theta)$ (*top left*) and $\Delta T_{wav}(\theta)$ (*top right*) profiles, are shown in blue for the unmasked coldest spots in 100,000 simulations. The 1 and 2σ contours for the masked coldest spots are marked as dashed and dotted black lines, respectively. The CS's $\Delta T(\theta)$ and $\Delta T_{wav}(\theta)$ are shown (measured on Planck's SMICA map) as the dark blue dashed line. The subtle shift in the unmasked $\Delta T(\theta)$ profile around $\theta < 5^\circ$ shown on the *left* panel appears to lead to colder final temperatures shown on the *right* panel. The difference between the mean of the unmasked and masked ΔT (*left*) and ΔT_{wav} (*right*) profiles are indicated with a superscript $\mathcal{U}$ and $\mathcal{M}$, respectively, in the bottom panels.

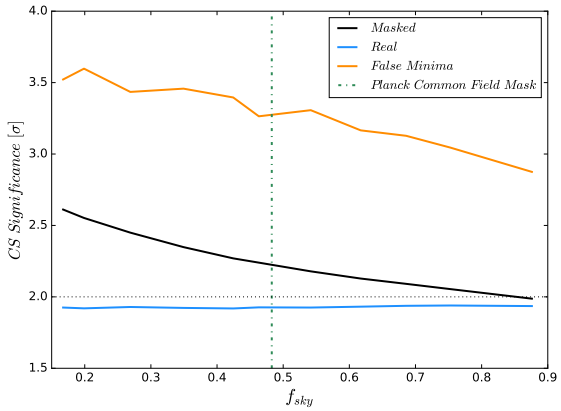

Figure 4. The significance of the CS is measured in comparison to the masked coldest spots (shown in black) as a function of the mask size (f_{sky} = unmasked fraction of the sky). In orange and blue the significance of the CS in comparison to false minima and real/unmasked coldest spots, respectively, is shown. This illustrates that the CS is found to be more significant due to the inclusion of false minima. The horizontal green dash-dotted line indicates the f_{sky} of the Planck Common Field mask.

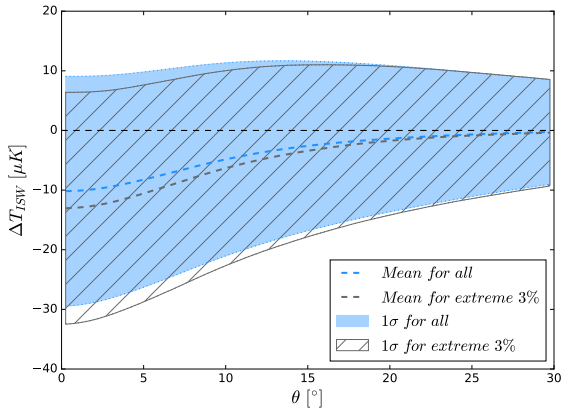

Figure 5. The 1σ contours of the ISW of all the unmasked coldest spots is shown in blue. The most extreme 3% are indicated by the grey hatched area. The mean for all the coldest spots and the most extreme 3% is indicated by the blue and grey dashed lines, respectively. The ISW in either case is not very well constrained and consistent with zero but on average appears to contribute $\sim 10\%$ to the coldest spots' profiles.

by Planck Collaboration et al. (2015a). However, our conclusions for the CS significance may not necessarily hold true for other angular scales. To test whether this is true for other angular scales R is varied between 4° and 7°, roughly equaling the range of R that Zhang & Huterer (2010) found the CS significant. The same procedure is carried out as before except with a smaller number of realisations (10,000).

In table 1 we summarise these results. The probability, $\mathbb{P}(\mathcal{U})$, is roughly equal to the fraction of unmasked pixels of the effective mask. However, the conditional probability $\mathbb{P}(\mathcal{U}|\mathcal{T}_\Psi^{CS})$ is found to be > 0.85 for the angular scales considered. When the unmasked significance $> 2\sigma$ the probability is even higher (> 0.93). This makes it appropriate to compare the CS to the unmasked coldest spots in simulations where it is $< 2\sigma$ for $4^\circ < R < 7^\circ$. Combined with previous studies (e.g. Vielva et al. 2004) means this holds true for all angular scales.

4 CONCLUSIONS

We measure the masked and the unmasked coldest spots in 100,000 simulations using the Planck Common Field mask which has a similar f_{sky} to the WMAP KQ75 and Planck U74 mask used in Zhang & Huterer (2010) and Nadathur et al. (2014), respectively. The probability of observing the

Table 1. The probability that the unmasked and masked coldest spot are equivalent for any $\Delta\mathcal{T}_\Psi$ and for the CS's $\Delta\mathcal{T}_\Psi^{CS}$ is indicated by $\mathbb{P}(\mathcal{U})$ and $\mathbb{P}\left(\mathcal{U}|\Delta\mathcal{T}_\Psi^{CS}\right)$, respectively, for each angular scale R. The significance of the CS is shown in comparison to the masked and unmasked coldest spots in CMB realisations. For each value of R (except $R = 5$ where 100,000 realisation were previously made) 10,000 CMB realisations were simulated.

R [°]	$\mathbb{P}(\mathcal{U})$	$\mathbb{P}\left(\mathcal{U}\|\Delta\mathcal{T}_\Psi^{CS}\right)$	Masked [σ]	Unmasked [σ]
4	0.51	0.94	1.95	1.65
4.5	0.50	0.96	2.18	1.85
5	**0.48**	**0.94**	**2.19**	**1.91**
5.5	0.46	0.96	2.19	1.89
6	0.45	0.94	2.08	1.76
6.5	0.44	0.91	1.85	1.50
7	0.42	0.86	1.53	1.13

unmasked coldest spot is found to be ~ 0.48 (roughly equaling the unmasked fraction of the effective mask). At other times we observe a false minima which biases the distribution (see figure 2). These false minima only appear to have a significant effect at $\Delta\mathcal{T}_\Psi > -18\mu K$ but at the CS's $\Delta\mathcal{T}_\Psi \simeq -19.3\mu K$ there is a ~ 0.94 probability that we are observing the CMB's unmasked coldest spot.

We argue that the CS is detected as an anomaly, with a significance of $\sim 2.2\sigma$, due to the inclusion of false minima when using a mask. Correcting for this bias, by comparing to the unmasked coldest spots, the significance is $\sim 1.9\sigma$. The difference in $\Delta T(\theta)$ and $\Delta T_{wav}(\theta)$ of the masked and unmasked coldest spots is subtle (see figure 3). But, a colder $\Delta T(\theta)$ for $\theta < 5°$ results in colder $\Delta\mathcal{T}_\Psi$. This result is true for all angular scales (see table 1) and would presumably remain for any model that can reproduce the CMB temperature C_ℓ. In this sense these results are model independent.

By varying the size of the mask the CS's significance is shown to be driven by the inclusion of false minima. The CS can only be considered an anomaly if it is a false minimum itself. This would require that a more extreme feature lies within the mask. This is unlikely, since such features are not seen in maps with a smaller mask or full sky reconstructed maps (Rassat et al. 2014).

We investigate the ISW contribution predicted by ΛCDM to the coldest spots finding it to be poorly constrained and consistent with zero, but leaning towards a negative contribution (see figure 5). On average it amounts to $\sim 10\%$ of the full profile. Measurements of large voids in the LOS and ISW reconstructions are consistent with this result. Since reconstructed ISW profiles (see Nadathur et al. 2014; Finelli et al. 2016; Kovács & García-Bellido 2016) appear to be below the mean shown in figure 5, it is possible that the ISW is amplifying the significance of the CS. This would mean the primordial CS profile is even less significant than measured. Alternative models, which are not investigated here, may better explain the slightly higher than expected causal relation between the ISW and large voids. Whether this is the case could be studied in future and would have implications for the predicted ISW contribution to the CS.

In this paper we have demonstrated the importance of understanding the bias masking, which is often unavoidable, can introduce on the analysis of CMB anomalies. It is important that this is accounted for in future studies.

ACKNOWLEDGEMENTS

We thank András Kovács, Seshadri Nadathur and Robert Crittenden for stimulating discussions. We also thank Andrew Pontzen, András Kovács, Juan García-Bellido and Seshadri Nadathur for providing useful comments and suggestions which helped improve the paper. KN acknowledges support from the Science and Technology Facilities Council grant ST/N50449X. ABL thanks CNES for financial support through its post-doctoral programme. OL acknowledges support from a European Research Council Advanced Grant FP7/291329. Some of the results were derived using the HEALPIX (Górski et al. 2005) package.

REFERENCES

Bennett C. L., et al., 2011, ApJS, 192, 17
Blas D., Lesgourgues J., Tram T., 2011, J. Cosmology Astropart. Phys., 7, 034
Bobin J., Sureau F., Starck J.-L., Rassat A., Paykari P., 2014, A&A, 563, A105
Bremer M. N., Silk J., Davies L. J. M., Lehnert M. D., 2010, MNRAS, 404, L69
Cai Y.-C., Neyrinck M. C., Szapudi I., Cole S., Frenk C. S., 2014, ApJ, 786, 110
Cayón L., Sanz J. L., Martínez-González E., Banday A. J., Argüeso F., Gallegos J. E., Górski K. M., Hinshaw G., 2001, MNRAS, 326, 1243
Cruz M., Cayón L., Martínez-González E., Vielva P., Jin J., 2007, ApJ, 655, 11
Finelli F., García-Bellido J., Kovács A., Paci F., Szapudi I., 2016, MNRAS, 455, 1246
Górski K. M., Hivon E., Banday A. J., Wandelt B. D., Hansen F. K., Reinecke M., Bartelmann M., 2005, ApJ, 622, 759
Granett B. R., Neyrinck M. C., Szapudi I., 2008, ApJ, 683, L99
Granett B. R., Szapudi I., Neyrinck M. C., 2010, ApJ, 714, 825
Hotchkiss S., Nadathur S., Gottlöber S., Iliev I. T., Knebe A., Watson W. A., Yepes G., 2015, MNRAS, 446, 1321
Ilić S., Langer M., Douspis M., 2013, A&A, 556, A51
Inoue K. T., Silk J., 2006, ApJ, 648, 23
Inoue K. T., Silk J., 2007, ApJ, 664, 650
Kovács A., 2017, preprint, (arXiv:1701.08583)
Kovács A., García-Bellido J., 2016, MNRAS, 462, 1882
Kovács A., et al., 2017, MNRAS, 465, 4166
Marcos-Caballero A., Fernández-Cobos R., Martínez-González E., Vielva P., 2016, MNRAS, 460, L15
Nadathur S., Crittenden R., 2016, ApJ, 830, L19
Nadathur S., Lavinto M., Hotchkiss S., Räsänen S., 2014, Phys. Rev. D, 90, 103510
Naidoo K., Benoit-Lévy A., Lahav O., 2016, MNRAS, 459, L71
Planck Collaboration et al., 2015b, preprint, (arXiv:1502.01589)
Planck Collaboration et al., 2015a, preprint, (arXiv:1506.07135)
Planck Collaboration et al., 2016, A&A, 594, A21
Rassat A., Starck J.-L., Paykari P., Sureau F., Bobin J., 2014, J. Cosmology Astropart. Phys., 8, 006
Rees M. J., Sciama D. W., 1968, Nature, 217, 511
Rogers K. K., Peiris H. V., Leistedt B., McEwen J. D., Pontzen A., 2016, MNRAS, 460, 3014
Sachs R. K., Wolfe A. M., 1967, ApJ, 147, 73
Szapudi I., et al., 2015, MNRAS, 450, 288
Vielva P., Martínez-González E., Barreiro R. B., Sanz J. L., Cayón L., 2004, ApJ, 609, 22
Zhang R., Huterer D., 2010, Astroparticle Physics, 33, 69
Zibin J. P., 2014, preprint, (arXiv:1408.4442)